Synchronization in an optomechanical cavity

Keren Shlomi, D. Yuvaraj, Ilya Baskin, Oren Suchoi, Roni Winik, and Eyal Buks
Department of Electrical Engineering, Technion, Haifa 32000, Israel
(Received 5 October 2014; published 13 March 2015)

We study self-excited oscillations (SEO) in an on-fiber optomechanical cavity. Synchronization is observed when the optical power that is injected into the cavity is periodically modulated. A theoretical analysis based on the Fokker-Planck equation evaluates the expected phase space distribution (PSD) of the self-oscillating mechanical resonator. A tomography technique is employed for extracting PSD from the measured reflected optical power. Time-resolved state tomography measurements are performed to study phase diffusion and phase locking of the SEO. The detuning region inside which synchronization occurs is experimentally determined and the results are compared with the theoretical prediction.

DOI: 10.1103/PhysRevE.91.032910 PACS number(s): 05.45.−a

I. INTRODUCTION

Optomechanical cavities [1–7] are widely employed for various sensing [8–11] and photonics applications [12–18]. Moreover, such systems may allow experimental study of the crossover between classical to quantum realms [2,19–28]. The effect of radiation pressure typically governs the optomechanical coupling (i.e., the coupling between the electromagnetic cavity and the mechanical resonator that serves as a movable mirror) when the finesse of the optical cavity is sufficiently high [2,4,27,29–31], whereas, bolometric effects can contribute to the optomechanical coupling when optical absorption by the vibrating mirror is significant [3,32–39]. Generally, bolometric effects are dominant in systems comprising of relatively large mirrors in which the thermal relaxation rate is comparable to the mechanical resonance frequency [36–38,40]. These systems [3,32,34,40–42] exhibit many intriguing phenomena such as mode cooling and self-excited oscillations (SEO) [1,28,34,37,40,43–45]. It has been recently demonstrated that optomechanical cavities can be fabricated on the tip of an optical fiber [46–55]. These micron-scale devices, which can be optically actuated [56], can be used for sensing physical parameters that affect the mechanical properties of the suspended mirror (e.g., absorbed mass, heating by external radiation, acceleration, etc.).

In the present study we optically induce SEO [8–11] by injecting a monochromatic laser light into an on-fiber optomechanical cavity, which is formed between a fiber Bragg grating (FBG) mirror, serving as a static reflector, and a vibrating mirror, which is fabricated on the tip of a single mode optical fiber. These optically induced SEO are attributed to the bolometric optomechanical coupling between the optical mode and the mechanical resonator [41,42]. We find that the phase of the SEO can be synchronized by periodically modulating the laser power that is injected into the cavity.

Synchronization [57], one of the most fundamental phenomena in nature, has been observed since 1673 [58] in many different setups and applications [59–64]. Synchronization in self-oscillating systems [65–71] can be the result of interaction between systems [72–78], external noise [79–86], or other outside sources, periodic [87–89] or non-periodic [90,91]. Synchronization can also be activated by delayed feedback [92–95].

Here we employ the technique of state tomography [53,96] in order to experimentally measure the phase space distribution (PSD) of the mechanical element near the threshold of SEO. Time resolved tomography [97] is employed in order to monitor the process of phase diffusion. Furthermore, we study the response of the system to periodic modulation of the laser power. We witness phase locking at certain regions of modulation amplitude and modulation frequency, for which the SEO are synchronized with the external modulation [98–103]. The experimental results are compared with theoretical predictions that are obtained by solving the Fokker-Planck equation that governs the dynamics of the system.

II. EXPERIMENTAL SETUP

The optomechanical cavity shown in Fig. 1 was fabricated on the flat polished tip of a single-mode fused silica optical fiber with outer diameter of 126 μm (Corning SMF-28 operating at wavelength band around 1550 nm) held in a zirconia ferrule (see Ref. [53]). A 10-nm-thick chromium layer and a 200 nm gold layer were successively deposited by thermal evaporation. The bilayer was directly patterned by a focused ion beam to the desired mirror shape (20-μm-wide doubly clamped beam). Finally, the mirror was released by etching approximately 12 μm of the underlying silica in 7% HF acid (90 min etch time at room temperature).

The static mirror of the optomechanical cavity was provided by a fiber Bragg grating (FBG) mirror (made using a standard phase mask technique [104], grating period of 0.527 μm and length ≈8 mm) with the reflectivity band of 0.4 nm full width at half-maximum (FWHM) centered at 1550 nm. The length of the optical cavity was $l \approx$10 mm, providing a free spectral range of $\Delta\lambda = \lambda_0^2/2n_{\text{eff}}l \approx 80$ pm (where $n_{\text{eff}} = 1.468$ is the effective refraction index for SMF-28). The cavity length was chosen so that at least five cavity resonance wavelengths would be located within the range of the FBG reflectivity band. Despite the high FBG reflectivity (≈90%), the resulting cavity finesse was low (about 2) due to the high cavity losses (see Ref. [41] for detailed discussion of the cavity reflectivity spectrum). The most plausible source of losses is the light scattering on the rough etched fiber tip surface (micron size protuberances were observed below the suspended beam), giving rise to radiation loss.

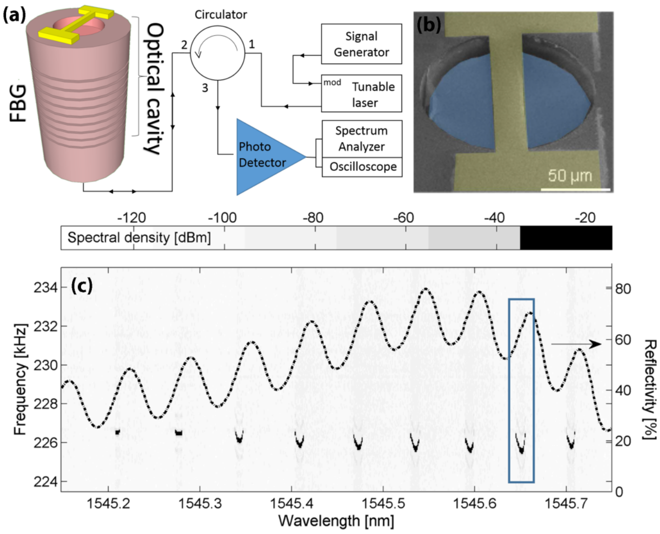

FIG. 1. (Color online) Experimental setup. (a) A schematic drawing of the sample and the experimental setup. An on-fiber optomechanical cavity is excited by a tunable laser with modulated power. The reflected light intensity is measured and analyzed. (b) Electron micrograph of a suspended micromechanical mirror (false color code: blue-silica fiber, yellow—gold mirror, gray—zirconia ferrule), the view is tilted by 52°. (c) Spectral decomposition of the reflected light power P_R vs. excitation wavelengths λ_L. The SEO, visible as sharp peaks (black regions on color map) in the reflected power spectrum, are obtained at optical excitation wavelengths corresponding to positive slopes of the sample's reflectivity (shown by a dotted curve). The cavity resonance used in the synchronization experiments is denoted by a rectangle.

Monochromatic light was injected into the fiber bearing the cavity on its tip from a laser source with an adjustable output wavelength (λ_L, tunable in the range of 1527.6–1565.5 nm) and power level P_L. The laser was connected through an optical circulator, that allowed the measurement of the reflected light intensity P_R by a fast responding photodetector. The detected signal was analyzed by an oscilloscope and a spectrum analyzer (see the schematics in Fig. 1). The experiments were performed in vacuum (at residual pressure below 0.01 Pa) at a base temperature of 77 K.

III. FOKKER-PLANCK EQUATION

The micromechanical mirror in the optical cavity is treated as a mechanical resonator with a single degree of freedom x having mass m and linear damping rate γ_0 (when it is decoupled from the optical cavity). It is assumed that the angular resonance frequency of the mechanical resonator depends on the temperature T of the suspended mirror. For small deviation of T from the base temperature T_0 (i.e., the temperature of the supporting substrate) it is taken to be given by $\omega_0 - \beta T_R$, where $T_R = T - T_0$ and where β is a constant. Furthermore, to model the effect of thermal deformation [34] it is assumed that a temperature dependent force given by $m\theta T_R$, where θ is a constant, acts on the mechanical resonator [39]. When noise is disregarded, the equation of motion governing the dynamics of the mechanical resonator is taken to be given by

$$\frac{d^2x}{dt^2} + 2\gamma_0\frac{dx}{dt} + (\omega_0 - \beta T_R)^2 x = \theta T_R. \tag{1}$$

The intracavity optical power incident on the suspended mirror is denoted by $P_L I(x)$, where P_L is the injected laser power, and the function $I(x)$ depends on the mechanical displacement x [see Eq. (3) below]. The time evolution of the relative temperature T_R is governed by the thermal balance equation

$$\frac{dT_R}{dt} = Q - \kappa T_R, \tag{2}$$

where $Q = \eta P_L I(x)$ is proportional to the heating power, η is the heating coefficient due to optical absorption, and κ is the thermal decay rate.

The function $I(x)$ depends on the properties of the optical cavity that is formed between the suspended mechanical mirror and the on-fiber static reflector. The finesse of the optical cavity is limited by loss mechanisms that give rise to optical energy leaking out of the cavity. The main escape routes are through the on-fiber static reflector, through absorption by the metallic mirror, and through radiation. The corresponding transmission probabilities are respectively denoted by $\mathcal{T}_B$, $\mathcal{T}_A$, and $\mathcal{T}_R$. In terms of these parameters, the function $I(x)$ is given by [41]

$$I(x) = \frac{\beta_F\left(1 - \frac{\beta_-^2}{\beta_+^2}\right)\beta_+^2}{1 - \cos\frac{4\pi x_D}{\lambda} + \beta_+^2}, \tag{3}$$

where $x_D = x - x_R$ is the displacement of the mirror relative to a point x_R, at which the energy stored in the optical cavity in steady state obtains a local maximum, $\beta_\pm^2 = (\mathcal{T}_B \pm \mathcal{T}_A \pm \mathcal{T}_R)^2/8$ and where β_F is the cavity finesse. The reflection probability $R_C = P_R/P_L$ is given in steady state by [41,105] $R_C = 1 - I(x)/\beta_F$. The function $I(x)$ can be expanded as $I(x) = I_0 + I_0' x + (1/2)I_0'' x^2 + O(x^3)$, where a prime denotes differentiation with respect to the displacement x.

Consider the case where the laser power P_L is periodically modulated in time according to

$$P_L = P_0 + P_1\cos(\omega_p t), \tag{4}$$

where P_0, P_1, and ω_p are constants. When both P_1 and $I - I_0$ are sufficiently small, the following approximation can be employed

$$Q = \eta P_L I \simeq \eta P_0 I + \eta P_1 I_0 \cos(\omega_p t). \tag{5}$$

For the case where $\kappa t \gg 1$, the solution of Eq. (2) can be expressed as

$$T_R = T_{R0} + T_{R1}, \tag{6}$$

where T_{R0} is a solution of Eq. (2) for the case where the laser power is taken to be the constant P_0, and where T_{R1}, which is given by

$$T_{R1} = \frac{\eta P_1 I_0 \cos(\omega_p t - \phi_p)}{\sqrt{\kappa^2 + \omega_p^2}}, \tag{7}$$

where $\tan\phi_p = \omega_p/\kappa$, represents the temperature variation due to the power modulation with a fixed displacement.

Substituting the expansion (6) into Eq. (1), neglecting terms of second order in β and disregarding the phase ϕ_p (i.e., shifting time by ϕ_p/ω_p) yield

$$\frac{d^2x}{dt^2} + 2\gamma_0\frac{dx}{dt} + \omega_m^2[1+\zeta\cos(\omega_p t)]x = f_{th} + f_e\cos(\omega_p t), \tag{8}$$

where $\omega_m^2 = \omega_0^2 - 2\omega_0\beta T_{R0}$ is the temperature dependent angular resonance frequency, $\zeta = -2\beta\eta P_l I_0/\omega_0\sqrt{\kappa^2+\omega_p^2}$ is the amplitude of parametric excitation due to laser power modulation [see Eq. (7)], $f_{th} = \theta T_{R0}$ is the thermal force, and $f_e = \theta\eta P_l I_0/\sqrt{\kappa^2+\omega_p^2}$ is the force amplitude due to laser power modulation [see Eq. (7)]. Furthermore, as was mentioned above, the temperature T_{R0} is assumed to satisfy [see Eq. (2)]

$$\frac{dT_{R0}}{dt} = \eta P_0 I(x) - \kappa T_{R0}. \tag{9}$$

As can be seen from Eq. (8), modulating the laser power gives rise to two contributions, one representing parametric excitation with amplitude ζ originating from the temperature dependence of the resonance frequency, and another representing direct forcing with amplitude f_e originating from the thermal force term. Both these terms can be treated using the rotating-wave approximation (RWA) only when the angular frequency ω_p is chosen to be close to particular values. Two such values are considered below, ω_0 and $2\omega_0$. When $\omega_p \simeq \omega_0$ the effect of the direct forcing term is expected to dominate, whereas when $\omega_p \simeq 2\omega_0$ the effect of the parametric term is expected to dominate. These two cases can be simultaneously treated by assuming that in Eq. (8) $\omega_p = \omega_0 + \omega_d$ in the direct forcing term and $\omega_p = 2(\omega_0 + \omega_d)$ in the parametric term, where $\omega_d \ll \omega_0$ is the detuning.

The displacement $x(t)$ can be expressed in terms of the complex amplitude A as $x(t) = x_0 + 2\,\mathrm{Re}(Ae^{i\omega_p t})$, where x_0, which is given by $x_0 = \eta\theta P_0 I_0/\kappa\omega_0^2$, is the optically induced static displacement. Assuming that A is small and it is slowly varying on the time scale of ω_0^{-1} and applying the RWA yield a first order evolution equation for the complex amplitude $A = A_x + iA_y$, where both A_x and A_y are real [42], which can be written in a vector form as

$$\dot{\mathbf{A}} + \mathbf{\Phi} = \boldsymbol{\xi}_R, \tag{10}$$

where $\mathbf{A} = (A_x, A_y)$, the vector $\mathbf{\Phi} = (\Phi_x, \Phi_y)$, where both Φ_x and Φ_y are real, is given by

$$\mathbf{\Phi} = \nabla\mathcal{H} + \omega_d(-A_y, A_x), \tag{11}$$

the scalar function $\mathcal{H}$ is given by [106]

$$\mathcal{H} = \frac{\Gamma_0(A_x^2+A_y^2)}{2} + \frac{\Gamma_2(A_x^2+A_y^2)^2}{4} + \frac{\omega_0\zeta}{4}A_xA_y - \frac{f_eA_x}{\omega_0}, \tag{12}$$

$\Gamma_0 = \gamma_0 + \eta\theta P_L I_0'/2\omega_0^2$ is the effective rate of linear damping, $\Gamma_2 = \gamma_2 + \eta\beta P_L I_0''/4\omega_0$ is the effective nonlinear quadratic damping rate, and γ_2 is the intrinsic mechanical contribution to Γ_2. The noise term $\boldsymbol{\xi}_R = (\xi_{Rx}, \xi_{Ry})$, where both ξ_{Rx} and ξ_{Ry} are real, satisfies $\langle\xi_{Rx}(t)\xi_{Rx}(t')\rangle = \langle\xi_{Ry}(t)\xi_{Ry}(t')\rangle = 2\tau\delta(t-t')$ and $\langle\xi_{Rx}(t)\xi_{Ry}(t')\rangle = 0$, where $\tau = \gamma_0 k_B T_{eff}/4m\omega_0^2$, k_B is the Boltzmann's constant and T_{eff} is the effective noise temperature.

In the absence of laser modulation, i.e., when $P_l = 0$, the equation of motion (10) describes a van der Pol oscillator [99]. Consider the case where $\Gamma_2 > 0$, for which a supercritical Hopf bifurcation occurs when the linear damping coefficient Γ_0 vanishes. Above threshold, i.e., when Γ_0 becomes negative, the amplitude $A_r = |A| = \sqrt{A_x^2 + A_y^2}$ of SEO is given by $A_{r0} = \sqrt{-\Gamma_0/\Gamma_2}$.

Consider the case of vanishing detuning, i.e., the case where $\omega_d = 0$, for which $\mathbf{\Phi} = \nabla\mathcal{H}$. For this case, the Langevin equation (10) for the complex amplitude A yields the corresponding Fokker-Planck equation for the PSD $\mathcal{P}(A_x, A_y)$, which can be written as [107,108]

$$\frac{\partial\mathcal{P}}{\partial t} - \nabla\cdot(\mathcal{P}\nabla\mathcal{H}) - \tau\nabla\cdot(\nabla\mathcal{P}) = 0. \tag{13}$$

IV. SYNCHRONIZATION

The steady-state solution $\mathcal{P}_0$ of (13) is given by [108]

$$\mathcal{P}_0 = \frac{1}{Z}\exp\left(-\frac{\mathcal{H}}{\tau}\right), \tag{14}$$

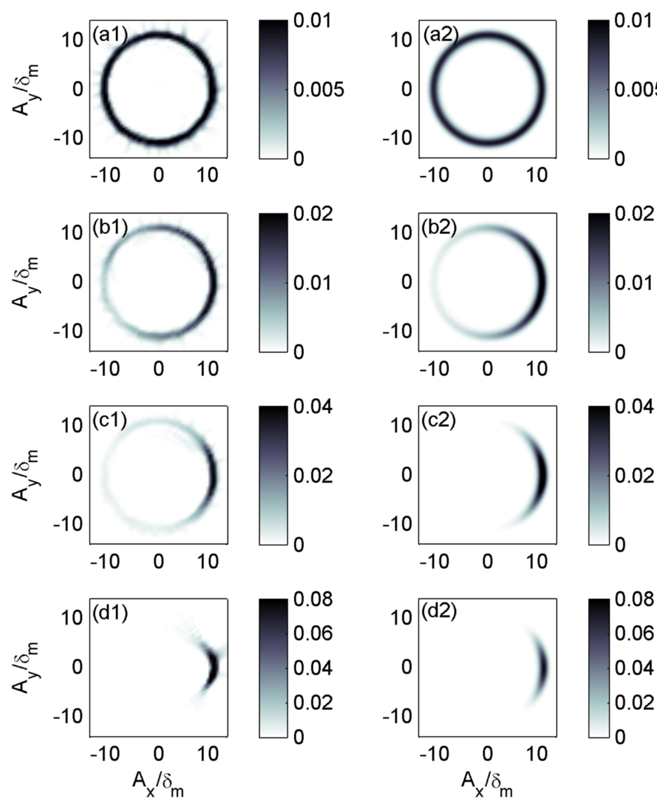

FIG. 2. (Color online) The PSD as a function of modulation amplitude at resonance $\omega_p = \omega_0$. The panels on the left exhibit the measured PSD whereas the panels on the right exhibit the calculated PSD obtained from Eq. (14). The modulation amplitude in (a), (b), (c), and (d) is $P_l/P_0 = 0.3\times10^{-3}$, 0.8×10^{-3}, 3.3×10^{-3}, and 6.7×10^{-3}, respectively. The following device parameters have been employed in order to calculate the PSD according to Eq. (14): $m = 1.1\times10^{-12}$ kg, $\omega_0 = 2\pi\times225$ kHz and $(I_0/I_0'\delta_m)(1+\kappa^2/\omega_p^2)^{-1/2} = 25$. The measured (calculated) normalized standard deviation σ_ϕ/σ_u for the distributions presented in (a)–(d) are 0.98 (0.98), 0.76 (0.60), 0.59 (0.25), and 0.08 (0.17), respectively.

where Z is a normalization constant (partition function). We experimentally investigate the effect of laser power modulation for the above discussed two cases, i.e., $\omega_p = \omega_0$ and $\omega_p = 2\omega_0$, and compare the results to the theoretical prediction given by Eq. (14) [recall that Eq. (14) is valid only when the detuning vanishes, i.e., when $\omega_d = 0$]. For both cases, the PSD is extracted from the measured off reflected cavity power using the technique of state tomography [53,96].

The results that are obtained with $\omega_p = \omega_0$ are seen in Fig. 2. For this case, the laser wavelength is $\lambda_L = 1545.641$ nm and the average power is $P_0 = 12$ mW (the data seen in Figs. 3, 4, and 5 was taken with the same values of λ_L and P_0). The panels on the left exhibit the measured PSD whereas the panels on the right exhibit the calculated PSD obtained from Eq. (14). The fitting parameters, i.e., the parameters that are not directly measured, are κ, θ, and β. For both cases, the PSD is plotted as a function of the normalized coordinates A_x/δ_m and A_y/δ_m, where $\delta_m = \sqrt{2\tau/\gamma_0}$. The relative modulation amplitude P_1/P_0 is increased from top to bottom (see figure caption for the values). The ring-like shape of the PSD, which is seen in the top panels, in which the relative modulation amplitude P_1/P_0 obtains its lowest value, changes into a crescent-like shape as P_1/P_0 is increased. While a PSD having a ring-like shape corresponds to SEO with a random phase, synchronization gives rise to a PSD having a crescent-like shape. The characteristic length of the crescent depends on both the modulation amplitude and the noise intensity in the system. The level of synchronization can be characterized by the normalized standard deviation σ_ϕ/σ_u, where σ_ϕ is the standard deviation of the phase ϕ of SEO and where $\sigma_u = 3^{-1/2}\pi$ is the value corresponding to uniform distribution. The device parameters that have been employed in the theoretical calculation are listed in the figure caption.

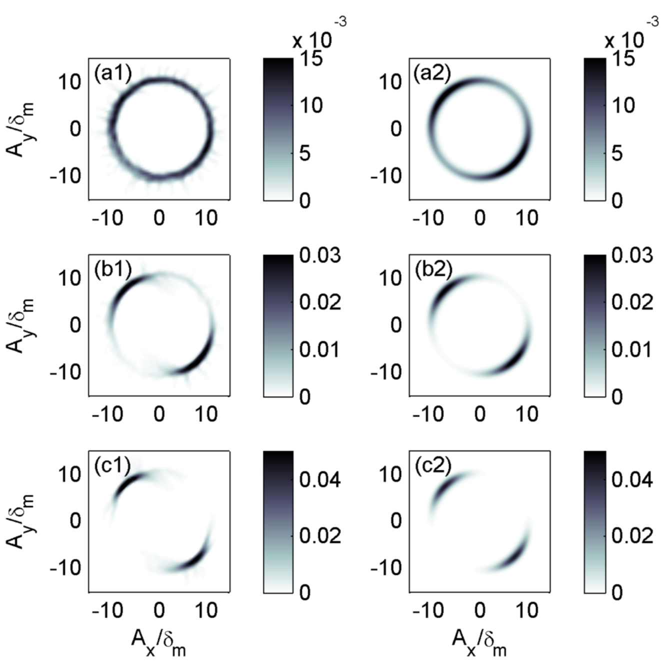

FIG. 3. (Color online) The PSD as a function of modulation amplitude at angular frequency $\omega_p = 2\omega_0$. The panels on the left exhibit the measured PSD whereas the panels on the right exhibit the calculated PSD obtained from Eq. (14). The modulation amplitude in (a), (b), and (c) is $P_1/P_0 = 0.67 \times 10^{-2}$, 2×10^{-2}, and 3.3×10^{-2}, respectively. The parameter $\lambda_L\beta\omega_0/\theta = 4800$ together with the other parameters that are listed in the caption of Fig. 2 have been employed in order to calculate the PSD according to Eq. (14). The measured (calculated) normalized standard deviation σ_ϕ/σ_u for the distributions presented in (a), (b), and (c) are 1.0 (0.99), 0.90 (0.92), and 0.88 (0.89), respectively.

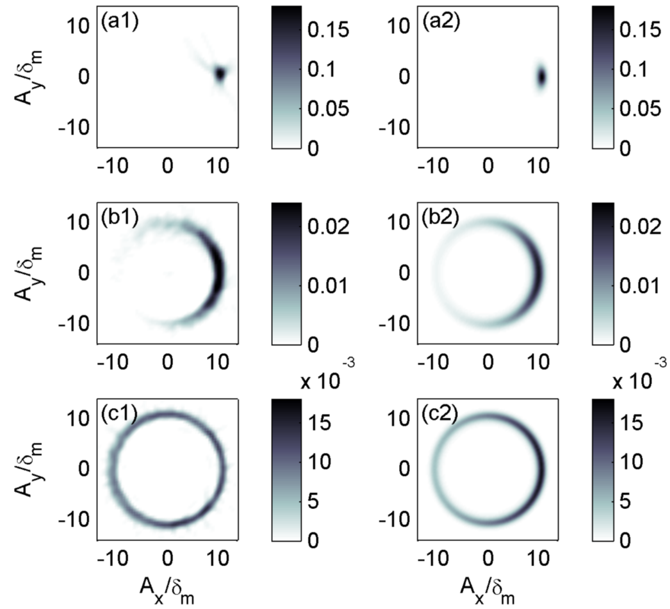

FIG. 4. (Color online) Dephasing of SEO. The panels on the left exhibit the measured PSD whereas the panels on the right exhibit the calculated PSD obtained from numerically integrating the Fokker-Planck equation (13). The normalized dwell time $\gamma_0 t_d$ in (a), (b), and (c) is $\gamma_0 t_d = 0.15$, 2.5, and 75, respectively. The device parameters are the same as those given in the caption of Fig. 2. The measured (calculated) normalized standard deviation σ_ϕ/σ_u for the distributions presented in (a), (b), and (c) are 0.04 (0.11), 0.48 (0.60), and 0.99 (0.83), respectively.

The results that are obtained with $\omega_p = 2\omega_0$ are seen in Fig. 3. The relative modulation amplitude P_1/P_0 is increased from top to bottom (see figure caption for the values). For this case of modulation at $\omega_p = 2\omega_0$, synchronization gives rise to two preferred values of the phase of SEO, which differ one from the other by π, as can be seen from the double-crescent shape of both measured and calculated PSD (see Fig. 3).

V. DEPHASING AND REPHASING

The phase of SEO in steady state randomly drifts in time due to the effect of external noise. In addition, noise gives rise to amplitude fluctuations around the average value A_{r0}. To experimentally study these effects, SEO are driven using the same parameters of laser power and wavelength as in Figs. 2 and 3. The off-reflected signal from the optical cavity is recorded in two time windows separated by a dwell time t_d. While the data taken in the first time window are used to determine the initial phase of SEO, the data taken in the second one are used to extract PSD by state tomography [53] using the initial phase as a reference phase. No modulation is applied in this experiment. The results are seen in Fig. 4 for

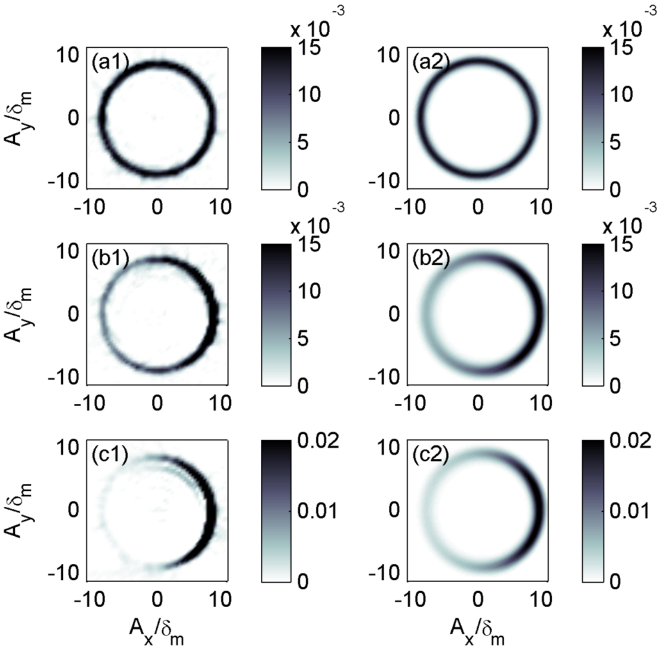

FIG. 5. (Color online) Rephasing of SEO. The relative amplitude of the modulation, which is turned on at time $t_0 = 1$ s after the first time window, is $P_1/P_0 = 0.01$. The normalized dwell time $\gamma_0 t_{\mathrm{d}}$ in (a), (b), and (c) is $\gamma_0 t_{\mathrm{d}} = 0.05$, 0.95, and 1.7, respectively. The device parameters are the same as those given in the caption of Fig. 2. The panels on the left exhibit the measured PSD whereas the panels on the right exhibit the calculated PSD obtained from numerically integrating the Fokker-Planck equation (13). The measured (calculated) normalized standard deviation $\sigma_\phi/\sigma_{\mathrm{u}}$ for the distributions presented in (a), (b), and (c) are 0.99 (1.0), 0.71 (0.80), and 0.39 (0.69), respectively.

three different values of the dwell time t_{d} (given in the figure caption). While the left panels show the measured PSDs, the panels on the right exhibit the calculated PSDs obtained by numerically integrating the Fokker-Planck equation (13). The process of dephasing of SEO is demonstrated by the transition from a PSD having a crescent-like shape that is obtained for a relatively short dwell time t_{d} (see top panels) to a PSD having a ring-like shape that is obtained for a relatively long dwell time t_{d} (see bottom panels).

The opposite process to dephasing, which is hereafter referred to as rephasing, is demonstrated in Fig. 5. As was done in the previous experiment, the off-reflected signal from the optical cavity is recorded in two time windows separated by a dwell time, which is labeled for the current case as $t_0 + t_{\mathrm{d}}$. In addition, power modulation at resonance (i.e., with $\omega_{\mathrm{p}} = \omega_0$) is turned on at time $t_0 = 1$ s after the first time window. The time t_0 is chosen to be much longer than the dephasing time, and consequently the phase of SEO is fully randomized at time t_0. While in Fig. 2 above, the case of synchronization in steady state, i.e., in the limit of $t_{\mathrm{d}} \to \infty$, is demonstrated, in the current experiment the PSD is measured for finite values of t_{d} in order the monitor in time the process of rephasing. Contrary to the case of dephasing (see Fig. 4), rephasing is demonstrated by the transition from a PSD having a ring-like shape that is obtained for a relatively short dwell time t_{d} (see top panels in Fig. 5) to a PSD having a crescent-like shape that is obtained for a relatively long dwell time t_{d} (see bottom panels).

VI. DETUNING RANGE OF PHASE LOCKING

The region in the plane of modulation frequency ω_{p} and modulation amplitude f_{e} in which synchronization occurs can be determined by finding the fixed points of Eq. (10) and by analyzing their stability [98,99]. Consider the case where $\omega_{\mathrm{p}} \simeq \omega_0$. For this case both the parametric term and the noise term are disregarded, and thus $\mathbf{\Phi} = (\Phi_x, \Phi_y)$ becomes [see Eq. (11)]

$$\Phi_x = \left[\Gamma_0 + \Gamma_2\left(A_x^2 + A_y^2\right)\right]A_x - \omega_{\mathrm{d}} A_y - f_{\mathrm{e}}, \tag{15}$$

$$\Phi_y = \left[\Gamma_0 + \Gamma_2\left(A_x^2 + A_y^2\right)\right]A_y + \omega_{\mathrm{d}} A_x. \tag{16}$$

At a fixed point, i.e., when $\Phi_x = \Phi_y = 0$, the following holds:

$$\mathcal{F}^2 = [(1 - \mathcal{A}^2)^2 + \mathcal{D}^2]\mathcal{A}^2, \tag{17}$$

where $\mathcal{F} = f_{\mathrm{e}}/A_{r0}\Gamma_0$ is the normalized modulation amplitude, $\mathcal{A} = A_r/A_{r0}$ is the normalized radial coordinate, $A_{r0} = \sqrt{-\Gamma_0/\Gamma_2}$ is the amplitude of SEO, and $\mathcal{D} = \omega_{\mathrm{d}}/\Gamma_0$ is the normalized detuning.

The Jacobian matrix is given by

$$J = \begin{pmatrix} \frac{\partial \Phi_x}{\partial A_x} & \frac{\partial \Phi_x}{\partial A_y} \\ \frac{\partial \Phi_y}{\partial A_x} & \frac{\partial \Phi_y}{\partial A_y} \end{pmatrix}. \tag{18}$$

The eigenvalues $\lambda_\pm$ of J can be expressed in terms of the trace $\operatorname{Tr} J = 2\Gamma_0(1 - 2\mathcal{A}^2)$ and determinant $\det J = \Gamma_0^2(3\mathcal{A}^4 - 4\mathcal{A}^2 + 1 + \mathcal{D}^2)$ of J as

$$\lambda_\pm = \frac{\operatorname{Tr} J \pm \sqrt{(\operatorname{Tr} J)^2 - 4\det J}}{2}. \tag{19}$$

Hopf bifurcation occurs when $\operatorname{Tr} J = 0$, i.e., when

$$\mathcal{A}^2 = \tfrac{1}{2}, \tag{20}$$

and when $\det J > 0$, i.e., when $\mathcal{A}^2 < \mathcal{A}_-^2$ or $\mathcal{A}^2 > \mathcal{A}_+^2$, where

$$\mathcal{A}_\pm^2 = \tfrac{2}{3} \pm \tfrac{1}{3}\sqrt{1 - 3\mathcal{D}^2}. \tag{21}$$

Hopf bifurcation is thus possible only when $|\mathcal{D}| > 0.5$ [see Eq. (20)]. Furthermore, combining Eqs. (17) and (20) yields a relation between the modulation amplitude $\mathcal{F}$ and the detuning $\mathcal{D}$ along the bifurcation line

$$8\mathcal{F}^2 = 1 + 4\mathcal{D}^2. \tag{22}$$

The critical value $\mathcal{F}_{\mathrm{c}}$ of $\mathcal{F}$ for which $\mathcal{D} = 0.5$ at the end of the bifurcation line is given by $\mathcal{F}_{\mathrm{c}} = 0.5$.

Steady-state bifurcation occurs when $\det J = 0$, i.e., when

$$0 = 3\mathcal{A}^4 - 4\mathcal{A}^2 + 1 + \mathcal{D}^2. \tag{23}$$

Substituting the solution, which is given by

$$\mathcal{A}_\pm^2 = \tfrac{2}{3} \pm \tfrac{1}{3}\sqrt{1 - 3\mathcal{D}^2}, \tag{24}$$

into Eq. (17) yields two branches

$$\mathcal{F}_\pm^2 = \left[\left(1 - \tfrac{2}{3} \mp \tfrac{1}{3}\sqrt{1 - 3\mathcal{D}^2}\right)^2 + \mathcal{D}^2\right]\left(\tfrac{2}{3} \pm \tfrac{1}{3}\sqrt{1 - 3\mathcal{D}^2}\right). \tag{25}$$

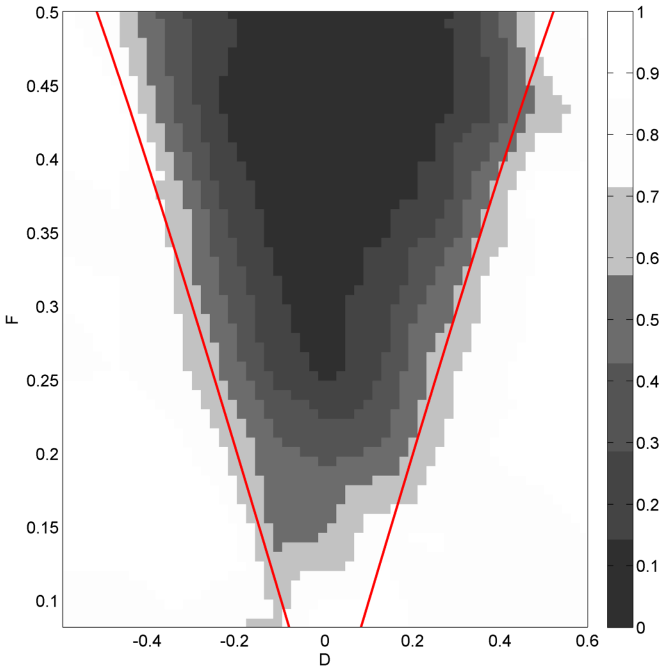

FIG. 6. (Color online) The normalized standard deviation σ_ϕ/σ_u vs. $\mathcal{D}$ and $\mathcal{F}$. The solid line is the steady state bifurcation line $\mathcal{F}_-(\mathcal{D})$ [see Eq. (25)]. The device parameters are the same as those given in the caption of Fig. 2.

Experimentally the region of synchronization is determined by measuring the standard deviation of the phase of SEO, which is labeled as σ_ϕ, with varying values of the normalized detuning $\mathcal{D}$ and normalized modulation amplitude $\mathcal{F}$. The measured normalized standard deviation σ_ϕ/σ_u is plotted in Fig. 6. In the region of phase locking, $\sigma_\phi/\sigma_u \ll 1$, whereas $\sigma_\phi/\sigma_u \simeq 1$ outside that region. The solid line is the steady-state bifurcation line $\mathcal{F}_-(\mathcal{D})$ [see Eq. (25)]. Theoretically, for $\mathcal{F} > \mathcal{F}_c = 0.5$ the region of phase locking is expected to be determined by the Hopf bifurcation line given by Eq. (22). However, this region is experimentally inaccessible with the laser used in our experiment due to limited range of modulation amplitude.

VII. SUMMARY

In summary, synchronization in an on-fiber optomechanical cavity is investigated. The relatively good agreement that is found between the experimental results and the theoretical predictions validates the assumptions and approximations that have been employed in the theoretical modeling. The investigated device can be employed as a sensor operating in the region of SEO. Future study will address the possibility of reducing phase noise by inducing synchronization in order to enhance the sensor's performance.

ACKNOWLEDGMENTS

This work was supported by the Israel Science Foundation, the bi-national science foundation, the Security Research Foundation in the Technion, the Israel Ministry of Science, the Russell Berrie Nanotechnology Institute, and MAGNET Metro 450 consortium.

[1] K. Hane and K. Suzuki, Self-excited vibration of a self-supporting thin film caused by laser irradiation, Sensors and Actuators A: Physical **51**, 179 (1996).
[2] S. Gigan, H. R. Böhm, M. Paternostro, F. Blaser, J. B. Hertzberg, K. C. Schwab, D. Bauerle, M. Aspelmeyer, and A. Zeilinger, Self cooling of a micromirror by radiation pressure, Nature **444**, 67 (2006).
[3] C. H. Metzger and K. Karrai, Cavity cooling of a microlever, Nature **432**, 1002 (2004).
[4] T. J. Kippenberg and K. J. Vahala, Cavity optomechanics: Back-action at the mesoscale, Science **321**, 1172 (2008).
[5] C. Metzger I. Favero, S. Camerer, D. Konig, H. Lorenz, J. P. Kotthaus, and K. Karrai, Optical cooling of a micromirror of wavelength size, Appl. Phys. Lett. **90**, 104101 (2007).
[6] Florian Marquardt and Steven M. Girvin, Optomechanics, Physics **2**, 40 (2009).
[7] V. Braginsky and A. Manukin, Ponderomotive effects of electromagnetic radiation, Sov. Phys. JETP **25**, 653 (1967).
[8] D. Rugar, H. J. Mamin, and P. Guethner, Improved fiber-optic interferometer for atomic force microscopy, Appl. Phys. Lett. **55**, 2588 (1989).
[9] O. Arcizet, P.-F. Cohadon, T. Briant, M. Pinard, A. Heidmann, J.-M. Mackowski, C. Michel, L. Pinard, O. Français, and L. Rousseau, High-sensitivity optical monitoring of a micromechanical resonator with a quantum-limited optomechanical sensor, Phys. Rev. Lett. **97**, 133601 (2006).
[10] S. Forstner, S. Prams, J. Knittel, E. D. van Ooijen, J. D. Swaim, G. I. Harris, A. Szorkovszky, W. P. Bowen, and H. Rubinsztein-Dunlop, Cavity optomechanical magnetometer, Phys. Rev. Lett. **108**, 120801 (2012).
[11] S. Stapfner, L. Ost, D. Hunger, J. Reichel, I. Favero, and E. M. Weig, Cavity-enhanced optical detection of carbon nanotube Brownian motion, Appl. Phys. Lett. **102**, 151910 (2013).
[12] S. E. Lyshevski and M. A. Lyshevski, Nano- and microoptoelectromechanical systems and nanoscale active optics, in *Third IEEE Conference on Nanotechnology* (IEEE, Piscataway, NJ, 2003), Vol. 2, pp. 840–843.
[13] N. A. D. Stokes, F. M. A. Fatah, and S. Venkatesh, Self-excited vibrations of optical microresonators, Electron. Lett. **24**, 777 (1988).
[14] M. Hossein-Zadeh and K. J. Vahala, An optomechanical oscillator on a silicon chip, IEEE J. Sel. Top. Quantum Electron. **16**, 276 (2010).
[15] M. C. Wu, O. Solgaard, and J. E. Ford, Optical MEMS for lightwave communication, J. Lightwave Technol. **24**, 4433 (2006).
[16] Matt Eichenfield, Christopher P. Michael, Raviv Perahia, and Oskar Painter, Actuation of micro-optomechanical systems via cavity-enhanced optical dipole forces, Nature Photonics **1**, 416 (2007).
[17] Gaurav Bahl, John Zehnpfennig, Matthew Tomes, and Tal Carmon, Stimulated optomechanical excitation of surface

acoustic waves in a microdevice, Nature Communications **2**, 403 (2011).

[18] N. E. Flowers-Jacobs, S. W. Hoch, J. C. Sankey, A. Kashkanova, A. M. Jayich, C. Deutsch, J. Reichel, and J. G. E. Harris, Fiber-cavity-based optomechanical device, Appl. Phys. Lett. **101**, 221109 (2012).

[19] J. D. Thompson, B. M. Zwickl, and A. M. Jayich, F. Marquardt, S. M. Girvin, and J. G. E. Harris, Strong dispersive coupling of a high-finesse cavity to a micromechanical membrane, Nature **452**, 72 (2008).

[20] Pierre Meystre, A short walk through quantum optomechanics, Ann. Phys. (Leipzig) **525**, 215 (2013).

[21] H. J. Kimble, Y. Levin, A. B. Matsko, K. S. Thorne, and S. P. Vyatchanin, Conversion of conventional gravitational-wave interferometers into quantum nondemolition interferometers by modifying their input and/or output optics, Phys. Rev. D **65**, 022002 (2001).

[22] A. M. Jayich, J. C. Sankey, B. M. Zwickl, C. Yang, J. D. Thompson, S. M. Girvin, A. A. Clerk, F. Marquardt, and J. G. E. Harris, Dispersive optomechanics: a membrane inside a cavity, New J. Phys. **10**, 095008 (2008).

[23] A. Schliesser, R. Riviere, G. Anetsberger, O. Arcizet, and T. J. Kippenberg, Resolved-sideband cooling of a micromechanical oscillator, Nat. Phys. **4**, 415 (2008).

[24] C. Genes, D. Vitali, P. Tombesi, S. Gigan, and M. Aspelmeyer, Ground-state cooling of a micromechanical oscillator: Comparing cold damping and cavity-assisted cooling schemes, Phys. Rev. A **77**, 033804 (2008).

[25] J. D. Teufel, D. Li, M. S. Allman, K. Cicak, A. J. Sirois, J. D. Whittaker, and R. W. Simmonds, Circuit cavity electromechanics in the strong-coupling regime, Nature **471**, 204 (2011).

[26] M. Poot and H. S. J. van der Zant, Mechanical systems in the quantum regime, Phys. Rep. **511**, 273 (2012).

[27] O. Arcizet, P.-F. Cohadon, T. Briant, M. Pinard, and A. Heidmann, Radiation-pressure cooling and optomechanical instability of a micromirror, Nature **444**, 71 (2006).

[28] T. Carmon, H. Rokhsari, L. Yang, T. J. Kippenberg, and K. J. Vahala, Temporal behavior of radiation-pressure-induced vibrations of an optical microcavity phonon mode, Phys. Rev. Lett. **94**, 223902 (2005).

[29] T. J. Kippenberg, H. Rokhsari, T. Carmon, A. Scherer, and K. J. Vahala, Analysis of radiation-pressure induced mechanical oscillation of an optical microcavity, Phys. Rev. Lett. **95**, 033901 (2005).

[30] H. Rokhsari, T. Kippenberg, T. Carmon, and K. J. Vahala, Radiation-pressure-driven micro-mechanical oscillator, Opt. Express **13**, 5293 (2005).

[31] Dustin Kleckner and Dirk Bouwmeester, Sub-kelvin optical cooling of a micromechanical resonator, Nature **444**, 75 (2006).

[32] G. Jourdan, F. Comin, and J. Chevrier, Mechanical mode dependence of bolometric backaction in an atomic force microscopy microlever, Phys. Rev. Lett. **101**, 133904 (2008).

[33] Francesco Marino and Francesco Marin, Chaotically spiking attractors in suspended-mirror optical cavities, Phys. Rev. E **83**, 015202 (2011).

[34] C. Metzger, M. Ludwig, C. Neuenhahn, A. Ortlieb, I. Favero, K. Karrai, and F. Marquardt, Self-induced oscillations in an optomechanical system driven by bolometric backaction, Phys. Rev. Lett. **101**, 133903 (2008).

[35] J. Restrepo, J. Gabelli, C. Ciuti, and I. Favero, Classical and quantum theory of photothermal cavity cooling of a mechanical oscillator, C. R. Phys. **12**, 860 (2011).

[36] S. D. Liberato, N. Lambert, and F. Nori, Quantum noise in photothermal cooling, Phys. Rev. A **83**, 033809 (2011).

[37] Florian Marquardt, J. G. E. Harris, and S. M. Girvin, Dynamical multistability induced by radiation pressure in high-finesse micromechanical optical cavities, Phys. Rev. Lett. **96**, 103901 (2006).

[38] M. Paternostro, S. Gigan, M. S. Kim, F. Blaser, H. R. Böhm, and M. Aspelmeyer, Reconstructing the dynamics of a movable mirror in a detuned optical cavity, New J. Phys. **8**, 107 (2006).

[39] D. Yuvaraj, M. B. Kadam, Oleg Shtempluck, and Eyal Buks, Optomechanical cavity with a buckled mirror, J. Microelectromech. Syst. **22**, 430 (2013).

[40] K. Aubin, M. Zalalutdinov, T. Alan, R. B. Reichenbach, R. Rand, A. Zehnder, J. Parpia, and H. Craighead, Limit cycle oscillations in CW laser-driven NEMS, J. Microelectromech. Syst. **13**, 1018 (2004).

[41] S. Zaitsev, A. K. Pandey, O. Shtempluck, and E. Buks, Forced and self-excited oscillations of optomechanical cavity, Phys. Rev. E **84**, 046605 (2011).

[42] S. Zaitsev, O. Gottlieb, and E. Buks, Nonlinear dynamics of a microelectromechanical mirror in an optical resonance cavity, Nonlinear Dyn. **69**, 1589 (2012).

[43] K. Kim and S. Lee, Self-oscillation mode induced in an atomic force microscope cantilever, J. Appl. Phys. **91**, 4715 (2002).

[44] Thomas Corbitt, David Ottaway, Edith Innerhofer, Jason Pelc, and Nergis Mavalvala, Measurement of radiation-pressure-induced optomechanical dynamics in a suspended fabry-perot cavity, Phys. Rev. A **74**, 021802 (2006).

[45] Tal Carmon and Kerry J. Vahala, Modal spectroscopy of optoexcited vibrations of a micron-scale on-chip resonator at greater than 1 ghz frequency, Phys. Rev. Lett. **98**, 123901 (2007).

[46] D. Iannuzzi, S. Deladi, V. J. Gadgil, R. G. P. Sanders, H. Schreuders, and M. C. Elwenspoek, Monolithic fiber-top sensor for critical environments and standard applications, Appl. Phys. Lett. **88**, 053501 (2006).

[47] Cheng Ma and Anbo Wang, Optical fiber tip acoustic resonator for hydrogen sensing, Opt. Lett. **35**, 2043 (2010).

[48] D. Chavan, G. Gruca, S. de Man, M. Slaman, J. H. Rector, K. Heeck, and D. Iannuzzi, Ferrule-top atomic force microscope, Rev. Sci. Instrum. **81**, 123702 (2010).

[49] Khashayar Babaei Gavan, Jan H. Rector, Kier Heeck, Dhwajal Chavan, Grzegorz Gruca, Tjerk H. Oosterkamp, and Davide Iannuzzi, Top-down approach to fiber-top cantilevers, Opt. Lett. **36**, 2898 (2011).

[50] Il Woong Jung, B. Park, J. Provine, R. T. Howe, and O. Solgaard, Highly sensitive monolithic silicon photonic crystal fiber tip sensor for simultaneous measurement of refractive index and temperature, J. Lightwave Technol. **29**, 1367 (2011).

[51] A. Butsch, M. S. Kang, T. G. Euser, J. R. Koehler, S. Rammler, R. Keding, and P. St. J. Russell, Optomechanical nonlinearity in dual-nanoweb structure suspended inside capillary fiber, Phys. Rev. Lett. **109**, 183904 (2012).

[52] Frank Albri, Jun Li, Robert R. J. Maier, William N. MacPherson, and Duncan P. Hand, Laser machining of sensing components on the end of optical fibres, Journal of Micromechanics and Microengineering **23**, 045021 (2013).

[53] Yuvaraj Dhayalan, Ilya Baskin, Keren Shlomi, and Eyal Buks, Phase space distribution near the self-excited oscillation threshold, Phys. Rev. Lett. **112**, 210403 (2014).
[54] A. B. Shkarin, N. E. Flowers-Jacobs, S. W. Hoch, A. D. Kashkanova, C. Deutsch, J. Reichel, and J. G. E. Harris, Optically mediated hybridization between two mechanical modes, Phys. Rev. Lett. **112**, 013602 (2014).
[55] Ilya Baskin, D. Yuvaraj, Gil Bachar, Keren Shlomi, Oleg Shtempluck, and Eyal Buks, Optically induced selfexcited oscillations in an On-fiber optomechanical cavity, JMEMS **23**, 563 (2014).
[56] G. Gruca, D. Chavan, J. Rector, K. Heeck, and D. Iannuzzi, Demonstration of an optically actuated ferrule-top device for pressure and humidity sensing, Sensors and Actuators A: Physical **190**, 77 (2013).
[57] Arkady Pikovsky, Michael Rosenblum, and Jürgen Kurths, A universal concept in nonlinear sciences, Self **2**, 3 (2001).
[58] C. Hugenii and Horoloqium Oscilatorium, The Pendulum Clock, *Trans RJ Blackwell, The Iowa State University Press, Ames*, 1986.
[59] Tat'yana Vilikovna Aulova, Nikolai Vladimirovich Kravtsov, Evgenii Grigor'evich Lariontsev, and Svetlana Nikolaevna Chekina, Quasi-periodic synchronisation of self-modulation oscillations in a ring chip laser by an external periodic signal, Quantum Electron. **41**, 504 (2011).
[60] Carsten Schäfer, Michael G. Rosenblum, Hans-Henning Abel, and Jürgen Kurths, Synchronization in the human cardiorespiratory system, Phys. Rev. E **60**, 857 (1999).
[61] Charles S. Peskin, *Mathematical aspects of heart physiology* (Courant Institute of Mathematical Sciences, New York University, New York, 1975).
[62] Frank Charles Hoppensteadt and Eugene M. Izhikevich, *Weakly connected neural networks*, Vol. 126 (Springer, New York, 1997).
[63] II Blekhman, Synchronization of dynamical systems, 1971.
[64] Iliya Izrailevich Blekhman, *Synchronization in science and technology* (American Society of Mechanical Engineers, 1988).
[65] Michael Rosenblum and Arkady Pikovsky, Synchronization: From pendulum clocks to chaotic lasers and chemical oscillators, Contemp. Phys. **44**, 401 (2003).
[66] Grigory V. Osipov, Jürgen Kurths, and Changsong Zhou, *Synchronization in oscillatory networks* (Springer, Berlin, 2007).
[67] Arkady Pikovsky, Michael Rosenblum, and Jürgen Kurths, Phase synchronization in regular and chaotic systems, Int. J. Bifurcation Chaos **10**, 2291 (2000).
[68] Valentin Senderovich Afraimovich, V. I. Nekorkin, G. V. Osipov, and A. V. Gaponov-Grekhov, *Stability, structures and chaos in nonlinear synchronization networks* (World Scientific, Singapore, 1994).
[69] Yu. I. Kuznetsov, P. S. Landa, A. F. Ol'Khovoi, and S. M. Perminov, Relationship between the amplitude threshold of synchronization and the entropy in stochastic self-excited systems, Soviet Physics Doklady **30**, 221 (1985).
[70] Polina S. Landa, *Regular and chaotic oscillations* (Springer, Berlin, 2001).
[71] Aleksandr Lvovich Fradkov and Alexander Yu Pogromsky, *Introduction to Control of Oscillations and Chaos*, Vol. 35 (World Scientific, Singapore, 1998).
[72] Louis M. Pecora and Thomas L. Carroll, Driving systems with chaotic signals, Phys. Rev. A **44**, 2374 (1991).
[73] Louis M. Pecora and Thomas L. Carroll, Synchronization in chaotic systems, Phys. Rev. Lett. **64**, 821 (1990).
[74] Maria de Sousa Vieira, Allan J. Lichtenberg, and Michael A. Lieberman, Synchronization of regular and chaotic systems, Phys. Rev. A **46**, R7359 (1992).
[75] Hirokazu Fujisaka and Tomoji Yamada, Stability theory of synchronized motion in coupled-oscillator systems, Prog. Theor. Phys. **69**, 32 (1983).
[76] P. S. Landa and M. G. Rosenblum, Synchronization and chaotization of oscillations in coupled self-oscillating systems, Appl. Mech. Rev. **46**, 414 (1993).
[77] Jerzy Warminski, Nonlinear normal modes of a self-excited system driven by parametric and external excitations, Nonlinear Dynamics **61**, 677 (2010).
[78] Marc-Antoine Lemonde, Nicolas Didier, and Aashish A. Clerk, Nonlinear interaction effects in a strongly driven optomechanical cavity, Phys. Rev. Lett. **111**, 053602 (2013).
[79] A. S. Pikovsky, Synchronization and stochastization of the ensamble of autogenerators by external noise, Radiophys. Quantum Electron. **27**, 576 (1984).
[80] A. G. Balanov, N. B. Janson, and P. V. E. McClintock, Coherence resonance of the noise-induced motion on the way to breakdown of synchronization in chaotic systems, Fluctuation and Noise Lett. **03**, L113 (2003).
[81] K. Czołczynski, P. Perlikowski, A. Stefański, and T. Kapitaniak, Synchronization of self-excited oscillators suspended on elastic structure, Chaos, Solitons & Fractals **32**, 937 (2007).
[82] A. G. Balanov, N. B. Janson, D. E. Postnov, and Peter V. E. McClintock, Coherence resonance versus synchronization in a periodically forced self-sustained system, Phys. Rev. E **65**, 041105 (2002).
[83] Xue-Juan Zhang and Guan-Xiang Wang, Stochastic resonance and signal recovery in two-dimensional arrays of coupled oscillators, Physica A: Statistical Mechanics and Applications **345**, 411 (2005).
[84] Michael G. Rosenblum, Arkady S. Pikovsky, and Jürgen Kurths, Phase synchronization of chaotic oscillators, Phys. Rev. Lett. **76**, 1804 (1996).
[85] Arkady S. Pikovsky, Michael G. Rosenblum, Grigory V. Osipov, and Jürgen Kurths, Phase synchronization of chaotic oscillators by external driving, Physica D: Nonlinear Phenomena **104**, 219 (1997).
[86] Y. T. Yang, C. Callegari, X. L. Feng, and M. L. Roukes, Surface adsorbate fluctuations and noise in nanoelectromechanical systems, Nano Lett. **11**, 1753 (2011).
[87] A. A. Koronovskii, M. K. Kurovskaya, and A. E. Hramov, Relationship between phase synchronization of chaotic oscillators and time scale synchronization, Tech. Phys. Lett. **31**, 847 (2005).
[88] Alexander P. Nikitin and Nigel G. Stocks, Estimation of periodicity in synchronised systems, in *Second International Symposium on Fluctuations and Noise* (International Society for Optics and Photonics, 2004), pp. 171–181.
[89] Qian Min and Zhang Xue-Juan, Frequency resonance in stochastic systems, Chin. Phys. Lett. **20**, 202 (2003).
[90] Seiichiro Nakabayashi and Kohei Uosaki, Synchronization of electrochemical oscillations with external perturbations, Chem. Phys. Lett. **217**, 163 (1994).

[91] Michael G. Rosenblum, Arkady S. Pikovsky, Jürgen Kurths, Grigory V. Osipov, István Z. Kiss, and John L. Hudson, Locking-based frequency measurement and synchronization of chaotic oscillators with complex dynamics, Phys. Rev. Lett. **89**, 264102 (2002).
[92] Natalia B. Janson, A. G. Balanov, and E. Schöll, Delayed feedback as a means of control of noise-induced motion, Phys. Rev. Lett. **93**, 010601 (2004).
[93] A. G. Balanov, Natalia B. Janson, and E. Schöll, Control of noise-induced oscillations by delayed feedback, Physica D: Nonlinear Phenomena **199**, 1 (2004).
[94] E. Schöll, A. G. Balanov, Natalia B. Janson, and A. Neiman, Controlling stochastic oscillations close to a hopf bifurcation by time-delayed feedback, Stochastics and Dynamics **05**, 281 (2005).
[95] Mustapha Hamdi and Mohamed Belhaq, Quasi-periodic oscillation envelopes and frequency locking in rapidly vibrated nonlinear systems with time delay, Nonlinear Dynamics **73**, 1 (2013).
[96] K. Vogel and H. Risken, Determination of quasiprobability distributions in terms of probability distributions for the rotated quadrature phase, Phys. Rev. A **40**, 2847 (1989).
[97] Oren Suchoi, Keren Shlomi, Lior Ella, and Eyal Buks, Time resolved phase space tomography of an optomechanical cavity, arXiv:1408.2331.
[98] V. S. Anishchenko and T. E. Vadivasova, Synchronization of self-oscillations and noise-induced oscillations, Journal of Communications Technology and Electronics C/C of Radiotekhnika i Elektronika **47**, 117 (2002).
[99] Manoj Pandey, Richard H. Rand, and Alan T. Zehnder, Frequency locking in a forced Mathieu–van der pol–Duffing system, Nonlinear Dynamics **54**, 3 (2008).
[100] L. J. Paciorek, Injection locking of oscillators, Proc. IEEE **53**, 1723 (1965).
[101] R. Adler, A study of locking phenomena in oscillators, Proc. IRE **34**, 351 (1946).
[102] M. Høgh Jensen, Per Bak, and Tomas Bohr, Complete devil's staircase, fractal dimension, and universality of mode-locking structure in the circle map, Phys. Rev. Lett. **50**, 1637 (1983).
[103] Serge Dos Santos and Michel Planat, Generation of 1/f noise in locked systems working in nonlinear mode, IEEE Trans. Ultrason. Ferroelectr. Freq. Control **47**, 1147 (2000).
[104] D. Z. Anderson, V. Mizrahi, T. Erdogan, and A. E. White, Production of in-fibre gratings using a diffractive optical element, Electron. Lett. **29**, 566 (1993).
[105] Bernard Yurke and Eyal Buks, Performance of cavity-parametric amplifiers, employing kerr nonlinearites, in the presence of two-photon loss, J. Lightwave Tech. **24**, 5054 (2006).
[106] S. Zaitsev, O. Shtempluck, E. Buks, and O. Gottlieb, Nonlinear damping in a micromechanical oscillator, Nonlinear Dynamics **67**, 859 (2012).
[107] Robert D. Hempstead and Melvin Lax, Classical noise. VI. Noise in self-sustained oscillators near threshold, Phys. Rev. **161**, 350 (1967).
[108] Hannes Risken, *The Fokker-Planck Equation: Methods of Solution and Applications* (Springer, Berlin, 1996).